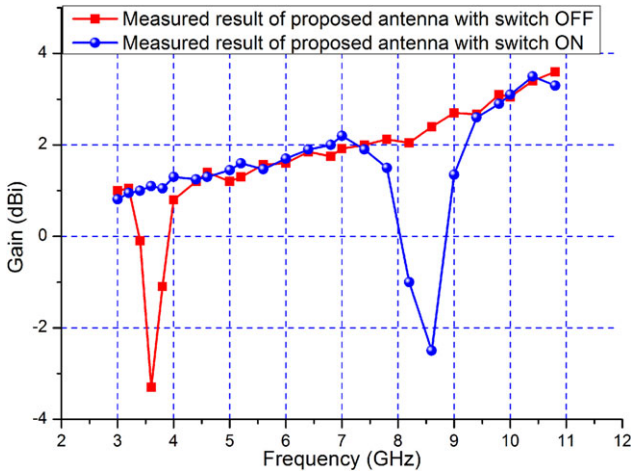

Figure 6 Gains of the fabricated reconfigurable antennas. [Color figure can be viewed in the online issue, which is available at wileyonlinelibrary.com]

4. CONCLUSION

An ACS-fed notch band reconfigurable UWB antenna using techniques of the staircase structure and the ideal switch is studied numerically and experimentally. The notch bands of the proposed antenna are obtained by using a spur-slot etched on the staircase radiation patch. The notch bands can be switched between 3.5-GHz WiMAX band and 8.2-GHz X-band by controlling the switch ON and OFF. The notch bands are also tunable by adjusting the total length of the spur-slot. Simulated and experimental results are analyzed and discussed. The proposed antenna, possessing a compact size and switchable notch band, is suitable for reconfigurable UWB communication applications.

ACKNOWLEDGMENTS

This work was partially supported by a grant from the National Defense "973" Basic Research Development Program of China (No. 6131380101). This article is also supported by the National Nature Science Fund of China (No. 60902014) and Nature Science Fund of Heilongjiang (QC2009C66). The authors are also thankful to Hebei VSTE Science and Technology Co., Ltd. for providing the measuring facility.

REFERENCES

1. P. Fei, Y.C. Jiao, Y. Zhu, and F.S. Zhang, Compact CPW-fed monopole antenna and miniaturized ACS-fed half monopole antenna for UWB applications, Microwave Opt Technol Lett 54 (2012), 1605–1609.
2. Y.S. Li, X.D. Yang, C.Y. Liu, and T. Jiang, Miniaturization cantor set fractal ultra-wideband antenna with a notch band characteristic, Microwave Opt Technol Lett 54 (2012), 1227–1230.
3. F. Fereidoony, S. Chamaani, and S.A. Mirtaheri, UWB monopole antenna with stable radiation pattern and low transient distortion, IEEE Antennas Wireless Propag Lett 10 (2011), 302–305.
4. H.R. Khaleel, H.M. Al-Rizzo, D.G. Rucker, and S. Mohan, A compact polyimide-based UWB antenna for flexible electronics, IEEE Antennas Wireless Propag Lett 11 (2012), 564–567.
5. S. Mohammadi, J. Nourinia, C. Ghobadi, and M. Majidzadeh, Compact CPW-fed rotated square-shaped patch slot antenna with band-notched function for UWB applications, Electron Lett 47 (2011), 1307–1308.
6. Q.X. Chu and Y.Y. Yang, 3.5/5.5 GHz dual band-notch ultra-wideband antenna, Electron Lett 44 (2008), 172–174.
7. C.Y. Hong, C.W. Ling, I.Y. Tam, and S.J. Chung, Design of a planar ultra-wideband antenna with a new band-notch structure, IEEE Trans Antennas Propag 55 (2012), 3391–3397.
8. Y.J. Cho, K.H. Kim, D.H. Choi, S.S. Lee, and S.O. Park, A miniature UWB planar monopole antenna with 5-GHz band-rejection filter and the time-domain characteristics, IEEE Trans Antennas Propag 54 (2006), 1453–1460.
9. C. Wang, Z.H. Yan, B. Li, and P. Xu, A dual band-notched UWB printed antenna with C-shaped and U-shaped slots, Microwave Opt Technol Lett 54 (2012), 1450–1452.
10. V. Deepu, R.K. Raj, M. Joseph, M.N. Suma, and P. Mohanan, Compact asymmetric coplanar strip fed monopole antenna for multiband applications, IEEE Trans Antennas Propag 55 (2007), 2351–2357.
11. P. Ashkarali, S. Sreenath, R. Sujith, R. Dinesh, D.D. Krishna, and C.K. Aanandan, A compact asymmetric coplanar strip fed dual-band antenna for DCS/WLAN applications, Microwave Opt Technol Lett 54 (2012), 1087–1089.
12. S. Soltani, M.N. Azarmanesh, and P. Lotfi, Design of small ACS-fed band-notch UWB monopole antenna using particle swarm optimization, Microwave Opt Technol Lett 52 (2010), 1510–1513.
13. Y. Li, W. Li, and R. Mittra, A cognitive radio antenna integrated with narrow/ultra-wideband antenna and switches, IEICE Electron Express 9 (2012), 1273–1283.
14. M.R. Hamid, P. Gardner, P.S. Hall, and F. Ghanem, Reconfigurable Vivaldi antenna, Microwave Opt Technol Lett 52 (2010), 785–786.

DECOUPLED WWAN/LTE ANTENNAS WITH AN ISOLATION RING STRIP EMBEDDED THEREBETWEEN FOR SMARTPHONE APPLICATION

Kin-Lu Wong, Po-Wei Lin, and Hung-Jen Hsu
Department of Electrical Engineering, National Sun Yat-sen University, Kaohsiung 80424, Taiwan; Corresponding author: wongkl@ema.ee.nsysu.edu.tw

Received 20 November 2012

ABSTRACT: *An integrated antenna array comprising two decoupled multiband WWAN/LTE antennas having an isolation ring strip embedded therebetween and all disposed on a same FR4 substrate of small size 10 × 70 mm^2 is presented. The two decoupled antennas cover the 824–960/1710–2690 MHz bands for the GSM850/900 and GSM1800/1900/UMTS/LTE2300/2500 operations and are promising to be mounted at the bottom edge of a smartphone for dual wireless wide area network (WWAN) operation for dual-talk function or for long term evolution (LTE) multiple-input multiple-output operation. The measured transmission coefficient S_{21} between the two antennas is less than −15 dB over both the 824–960 and 1710–2690 MHz bands, and the envelop correlation coefficient is less than about 0.03 over both bands. Port-decoupling of the two antennas is obtained because the excited surface currents on the system ground plane of the smartphone between the two antennas are decreased owing to the isolation ring strip attracting some of the same. In addition to good isolation obtained, the antenna efficiencies are better than about 40 and 50% over the lower and upper bands, respectively. Details of the decoupled WWAN/LTE antennas are described.* © 2013 Wiley Periodicals, Inc. Microwave Opt Technol Lett 55:1470–1476, 2013; View this article online at wileyonlinelibrary.com. DOI 10.1002/mop.27654

Key words: *handset antennas; mobile antennas; WWAN/LTE antennas; decoupled antennas; LTE MIMO antennas; dual WWAN operation*

1. INTRODUCTION

To provide dual wireless wide area network (WWAN) operation for dual-talk function or the long-term evolution (LTE) operation

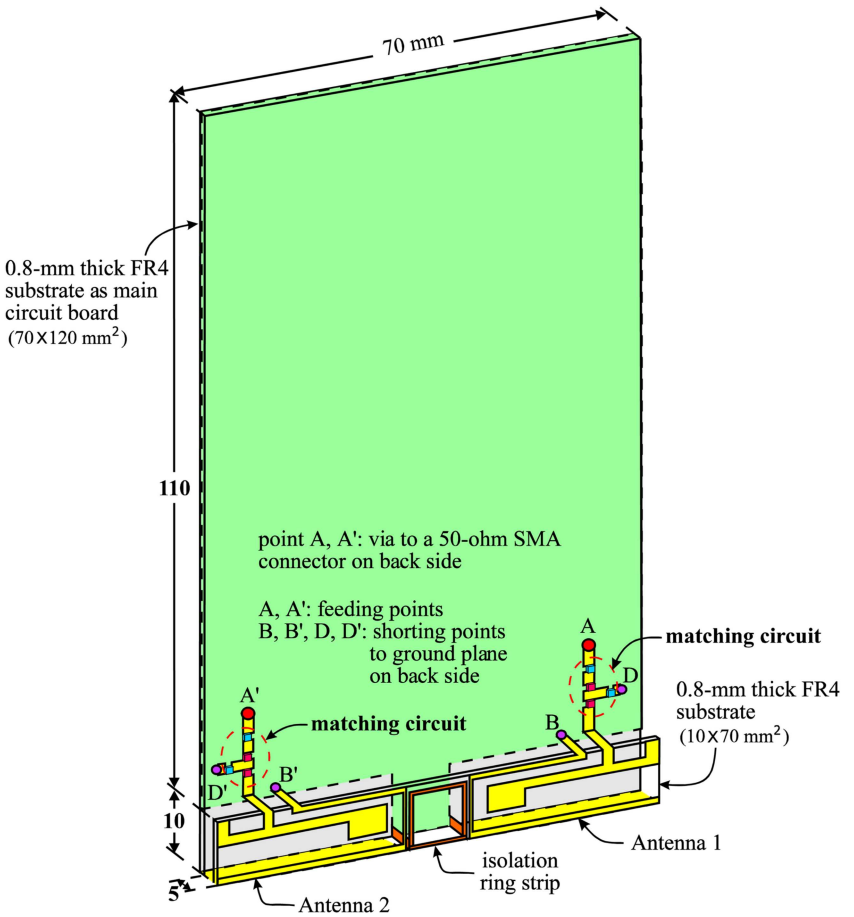

Figure 1 Geometry of an antenna array comprising two decoupled WWAN/LTE antennas with an isolation ring strip embedded therebetween and mounted at the bottom edge of the system circuit board of a smartphone. [Color figure can be viewed in the online issue, which is available at wileyonlinelibrary.com]

in the multiple-input multiple-output (MIMO) system in the handheld devices such as the smartphone, it is desired to have two small-size yet multiband antennas with enhanced isolation to be embedded in the limited space inside the handheld device. In this case, the two antennas are generally spaced close to each other. For such two closely spaced antennas to have enhanced isolation, the technique of using a neutralization line or a metallic suspended line connecting the two antennas therebetween to achieve enhanced isolation has been reported [1–4]. In Ref. 1, it is shown that the metallic suspended line leads to enhanced isolation between two mobile phone PIFAs operating in the different bands, such as the DCS 1800 and UMTS bands. While in Ref. 2, it is demonstrated that the metallic suspended line is able to operate like a band stop filter and leads to enhanced isolation between two feeding ports of the two closely spaced antennas in the LTE band class 13 (746–787 MHz). However, in the antenna's higher band (GSM1900/UMTS band), the isolation between the two feeding ports is still poor (S_{21} about -5 dB only). The suspended-line technique has also been applied to achieve enhanced isolation (S_{21} less than -12 dB) for two single-band handset MIMO antennas operating in the LTE700 band [3]. A similar technique of using a metallic line containing a chip inductor placed between two single-band handset MIMO antennas for LTE700 operation has also been reported in Ref. 4.

Isolation techniques reported for two closely spaced antennas also include using an LC-based branchline hybrid coupler to integrate with the antennas to decouple the ports [5], or using the metamaterial antennas to limit the excited surface currents in the system ground plane to thereby decrease the port coupling [6], or using the monopole antennas with magneto-dielectric materials [7], or using two antennas with ferrite materials [8]. The results obtained using these isolation techniques, however, are for single band or narrow band operation only. It is also noted that the radiation efficiency for the antennas using magneto-dielectric or ferrite materials is generally low (<30%) due to high material losses [7, 8].

In this article, an integrated antenna array comprising two decoupled multiband WWAN/LTE antennas having an isolation ring strip embedded therebetween and all disposed on a same FR4 substrate of small size 10×70 mm^2 is presented. The antenna array is to be mounted at the bottom edge of the system circuit board of a smartphone. In this case, it is expected that the antenna array can meet the SAR regulation for practical applications [9–12]. The two antennas in the antenna array are capable of covering the 824–960/1710–2690 MHz bands for the GSM850/900 and GSM1800/1900/UMTS/LTE2300/2500 operations and are suitable for dual WWAN operation for dual-talk function or for LTE MIMO operation. Owing to the embedded isolation ring strip which is short-circuited to the system ground plane of the smartphone, the excited surface currents on the system ground plane between the two antennas can be decreased because the ring strip can attract some of the same. This leads to enhanced isolation between the two antennas, and good isolation is obtained for frequencies over two wide operating bands.

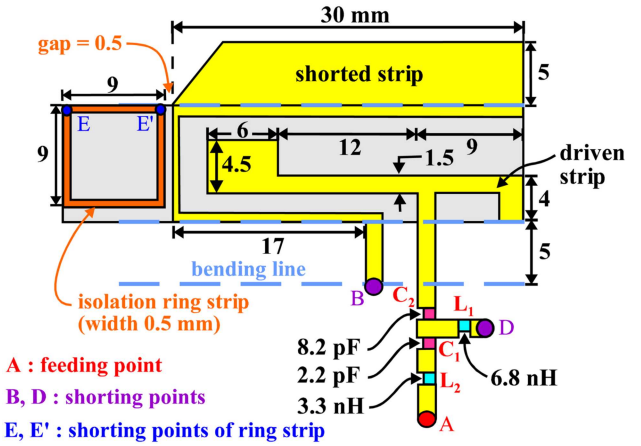

Figure 2 Dimensions of the WWAN/LTE antenna (antenna 1 in Fig. 1) and isolation ring strip. [Color figure can be viewed in the online issue, which is available at wileyonlinelibrary.com]

The measured transmission coefficient S_{21} between the two antennas in this study is less than −15 dB over both the 824–960 and 1710–2690 MHz bands, and the envelop correlation coefficient is less than about 0.03 over both bands. Each antenna also shows antenna efficiencies better than about 40 and 50% over its lower and upper bands, respectively. The proposed antenna array not only easy to implement on a small-size, thin FR4 substrate, and the two decoupled antennas therein shows good isolation and radiation efficiency over two wide operating bands. Details of the proposed WWAN/LTE antenna array are described, and the obtained results are presented and discussed.

2. PROPOSED ANTENNA ARRAY

Figure 1 shows the proposed antenna array comprising two decoupled WWAN/LTE antennas with an isolation ring strip embedded therebetween and mounted at the bottom edge of the system circuit board of a smartphone. The system circuit board in this study is an FR4 substrate of width 70 mm and length 120 mm. The two antennas (antenna 1, antenna 2) and the isolation ring strip are mainly disposed on a 0.8-mm thick FR4 substrate of size 10 × 70 mm^2. The antenna array is spaced above the system circuit board with a height of 5 mm. The configurations of antennas 1 and 2 are identical, and their dimensions are the same. Detailed dimensions of antenna 1 and isolation ring strip are given in Figure 2. Antenna 1 comprises a driven strip and a shorted strip, and the antenna volume is 10 × 30 × 5 mm^3 (1.5 cm^3 only). The antenna's lower band is mainly contributed by the fundamental or lowest resonant mode of the shorted strip. While the antenna's upper band is mainly contributed by the fundamental resonant mode of the driven strip, with the higher order resonant mode of the shorted strip generated to widen the operating bandwidth of the upper band. The lower and upper bands of the antenna cover the 824–960 and 1710–2690 MHz bands for the GSM850/900 and GSM1800/1900/UMTS/LTE2300/2500 operations, respectively.

Each antenna is also connected to a matching circuit comprising a high-pass matching circuit with L_1 (6.8 nH) and C_1 (2.2 pF), two reactance fine-tuning elements C_2 (8.2 pF) and L_2 (3.3 nH). The matching circuits help improve the impedance matching of the two antennas for frequencies over the lower and upper bands. Also note that the widened portion in the open end of the shorted strip is also helpful in achieving wider bandwidth of the two antennas. The widened portion is bent downward to

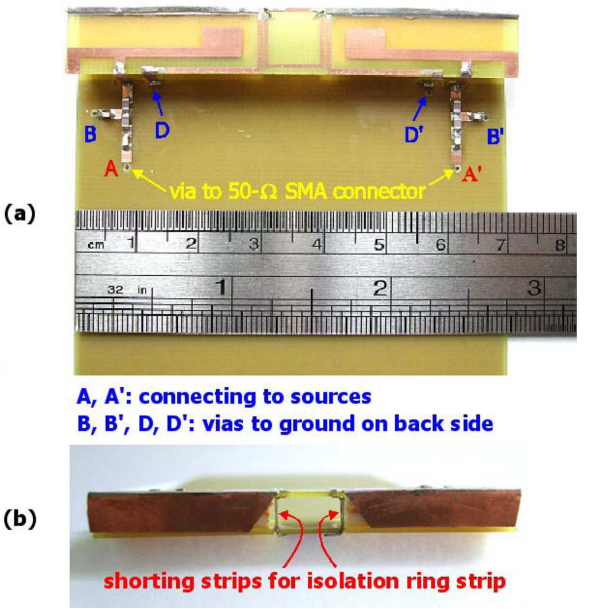

Figure 3 Photos of the fabricated antenna array prototype. (a) Top view. (b) Side view. [Color figure can be viewed in the online issue, which is available at wileyonlinelibrary.com]

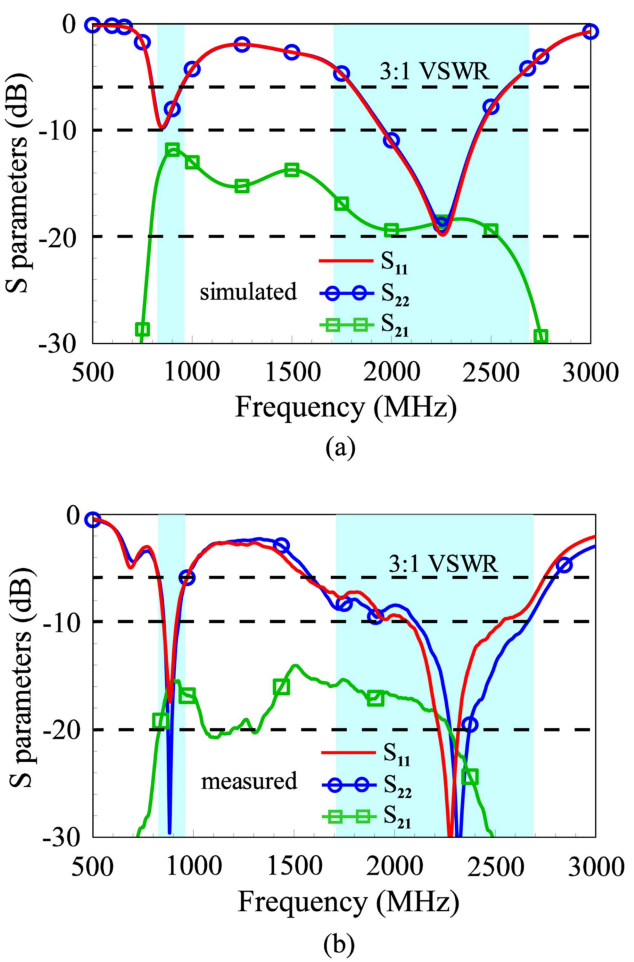

Figure 4 (a) Simulated and (b) measured S parameters of the two antennas in the proposed design. [Color figure can be viewed in the online issue, which is available at wileyonlinelibrary.com]

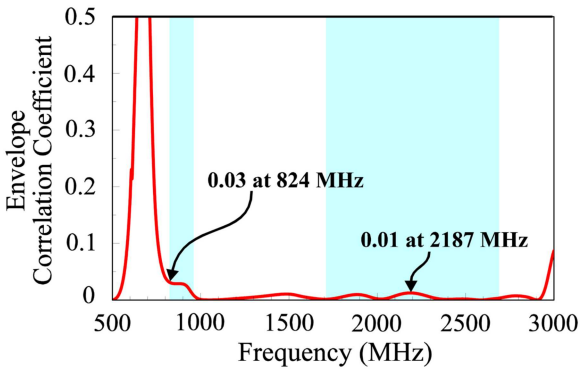

Figure 5 Envelop correlation coefficient ρ_e obtained from the measured S parameters in Figure 4. [Color figure can be viewed in the online issue, which is available at wileyonlinelibrary.com]

the system circuit board as seen in the photo of the fabricated antenna array shown in Figure 3.

The isolation ring strip having a width of 0.5 mm occupies an area of 9 × 9 mm^2 and is embedded between the two antennas, with a gap of 0.5 mm to antennas 1 and 2. The ring strip is short-circuited to a protruded ground (size 10 × 10 mm^2) at the bottom edge of the system ground plane printed on the system circuit board through two shorting strips. This protruded ground can be used to accommodate a universal series bus (USB) connector to serve as a data port for the smartphone [13–15]. In addition, this protruded ground can attract or detour some excited surface currents between the two antennas, which can result in isolation improvement between the two antennas for operating in the upper band [15].

However, for operating in the lower band, the protruded ground is not effective in attracting the excited surface currents between the two antennas, owing to its size not comparable to the wavelength of the frequencies in the lower band. With the proposed ring strip connected to the protruded ground, the combined structure can become effective in attracting some excited surface currents between the two antennas for operating in the upper band. This behavior leads to enhanced isolation for the two antennas in the proposed antenna array operating in the lower band. Further, the combined structure can result in enhanced isolation for operating in the upper band as well. By varying the size of the ring strip, the isolation behavior between the two antennas for frequencies over the lower and upper bands can be adjusted. In the proposed design, by selecting the size of the ring strip to be 9 × 9 mm^2, the measured transmission coefficient S_{21} between the two antennas can be less than about −15 dB over both the 824–960 and 1710–2690 MHz bands. Detailed results and the operating principle of the proposed antenna array for WWAN/LTE operation are presented in Section 3.

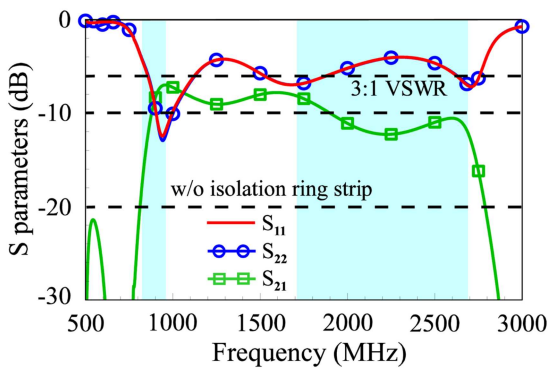

Figure 6 Simulated S parameters of the two antennas without the isolation ring strip. [Color figure can be viewed in the online issue, which is available at wileyonlinelibrary.com]

3. RESULTS AND DISCUSSION

The proposed antenna array was fabricated as shown in Figure 3. The simulated and measured S parameters of the two antennas are presented in Figure 4. The simulated results are obtained using the three-dimensional full-wave electromagnetic field simulator HFSS version 14 [16]. Agreement between the simulated results in Figure 4(a) and the measured data in Figure 4(b) is seen. Note that since the two antennas are of identical structures and dimensions, the measured S_{11} and S_{22} are about the same. Over the desired operating bands (shaded regions shown in figure for 824–960 and 1710–2690 MHz bands), the measured S_{11}

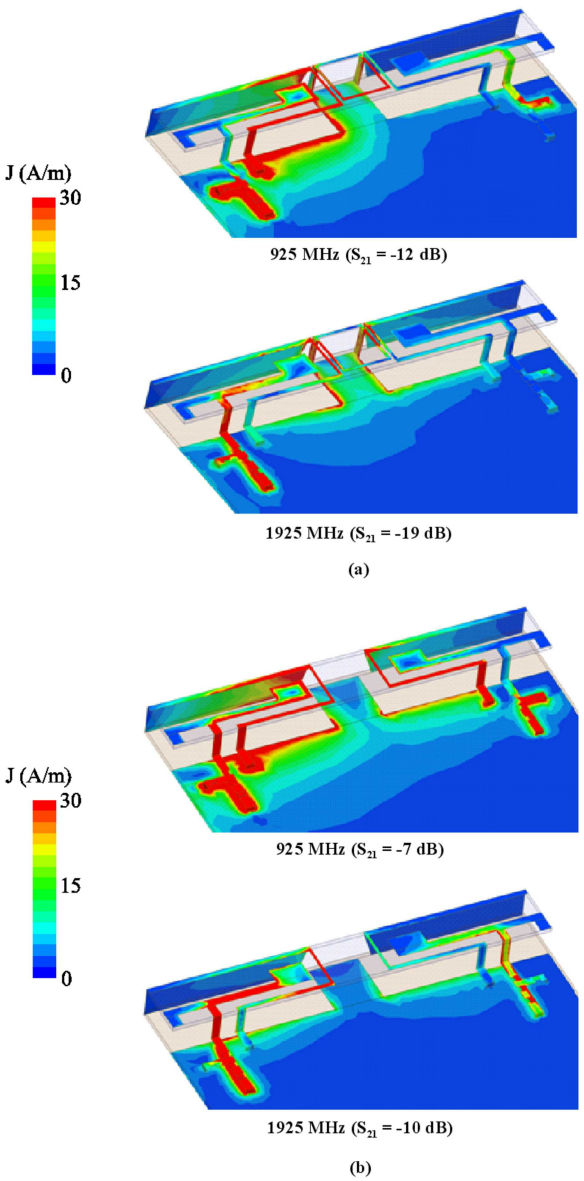

Figure 7 Simulated surface current distributions on the antennas and ground plane at 925 and 1925 MHz. (a) With the isolation ring strip. (b) Without the isolation ring strip. [Color figure can be viewed in the online issue, which is available at wileyonlinelibrary.com]

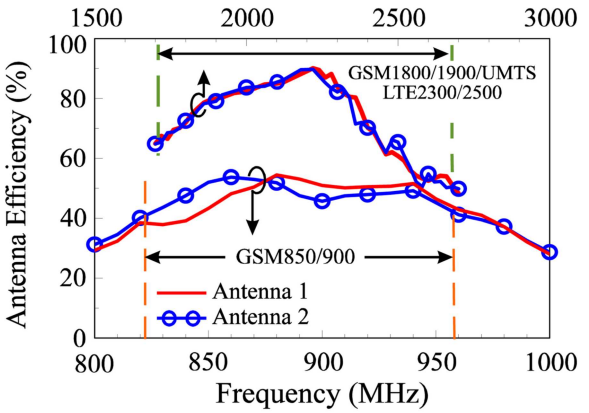

Figure 8 Measured antenna efficiency (mismatching losses included) for the two antennas in the proposed design. [Color figure can be viewed in the online issue, which is available at wileyonlinelibrary.com]

and S_{22} show impedance matching better than −6 dB, which is a widely used design specification for the smartphone WWAN/LTE antennas. For the measured S_{21}, it is seen to be less than −15 dB for frequencies over the lower and upper bands. The envelop correlation coefficient ρ_e obtained from the measured S parameters [15] in Figure 4 is also presented in Figure 5. The envelope correlation coefficient is very small, less than about 0.03 over the lower band and less than about 0.01 over the upper band, which is good for practical MIMO applications.

To analyze the effect of the ring strip between the two antennas, Figure 6 shows the simulated S parameters of the two antennas without the isolation ring strip. In this case, the two antennas are of the same dimensions as those studied in Figure 4. It is seen that the impedance matching for frequencies over the upper band is degraded, and the S_{21} is also quickly degraded. The S_{21} has a highest value of about −8 dB at 1710 MHz. It is expected that if the impedance matching is improved over the upper band, the S_{21} will be even degraded [6]. For the lower band, the operating band is seen to be slightly shifted to higher frequencies, and the highest S_{21} reaches about −7 dB. By comparing the results with those in Figure 4, it is evident that the ring strip is effective in decreasing the coupling between the two antennas.

The simulated surface current distributions on the antennas and ground plane at 925 and 1925 MHz are also analyzed. Results for the cases with and without the isolation ring strip are presented in Figures 7(a) and 7(b), respectively. Results are obtained with antenna 1 excited and antenna 2 terminated to 50 Ω. At 925 MHz, when there is no ring strip, the S_{21} is increased from −12 dB to −7 dB. Similarly, at 1925 MHz, the S_{21} is

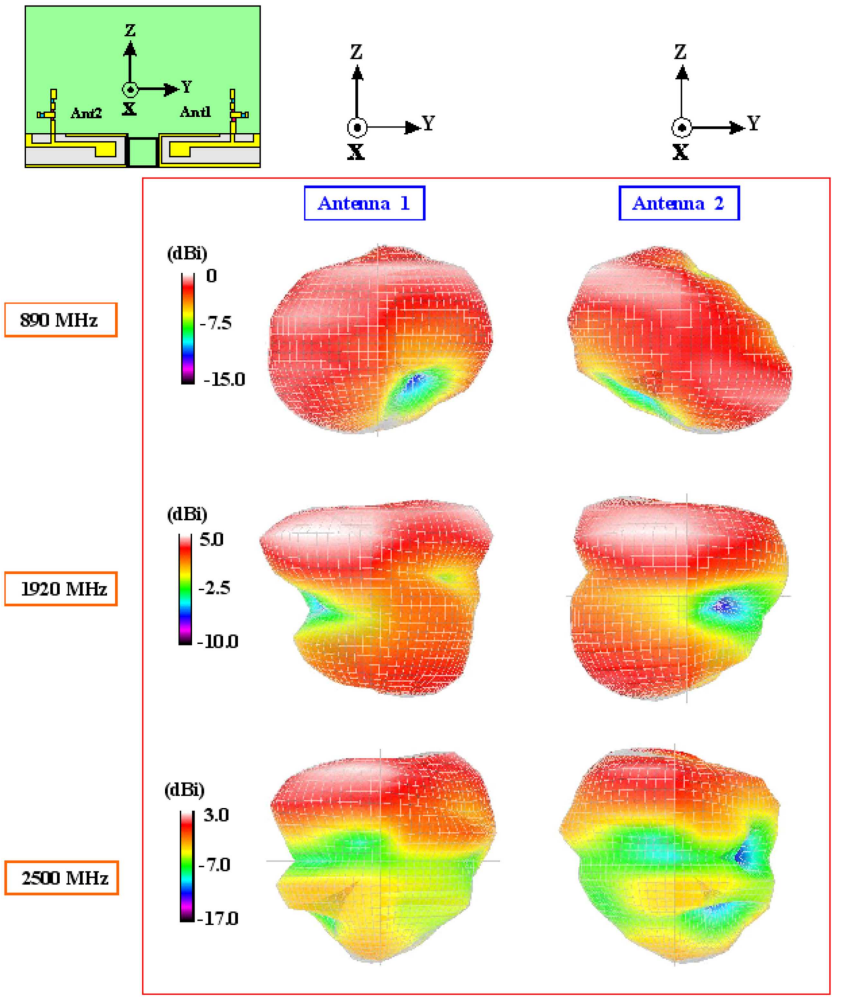

Figure 9 Measured radiation patterns of the two antennas in the proposed design. (a) Antenna 1. (b) Antenna 2. [Color figure can be viewed in the online issue, which is available at wileyonlinelibrary.com]

increased from −19 dB to −10 dB, when the ring strip is not present. For both frequencies, it can be seen that strong excited surface currents are directed to the protruded ground, which leads to decreased coupling between the two antennas.

Figure 8 shows the measured antenna efficiency for the two antennas in the proposed design. The measured antenna efficiency includes mismatching losses. For the lower band, the antenna efficiency of the two antennas is about 40–52%; whereas for the upper band, the antenna efficiency of the two antennas is about 50–90%. The measured three-dimensional radiation patterns of the two antennas at typical frequencies are plotted in Figure 9. At 890 MHz, asymmetric dipole-like radiation patterns for antennas 1 and 2 are seen. The asymmetry is owing to the presence of the protruded ground which attracts some excited surface currents. A higher frequencies (1920 and 2500 MHz in the figure), some dips are seen in the radiation patterns of antennas 1 and 2, which are owing to the current nulls of the excited surface currents on the system ground plane. Also, owing to similar structures of the two antennas, the radiation patterns of antenna 1 are seen to be symmetric to those of antenna 2 with respect to the central axis (z-axis) of the system ground plane. The obtained radiation characteristics are acceptable for practical applications.

Some parametric studies are also conducted. Figure 10 shows the simulated S parameters of the two antennas with the isolation ring strip of different sizes. Results for the length a of the ring strip varied from 6 to 10 mm are presented. Only S_{11} and S_{21} are shown. The simulated results of S_{22} are generally the same as those of S_{11} and are therefore not shown. Results for $a = 9$ and 10 mm are seen to be better than those of $a = 6$ mm. This behavior is simply because smaller size of the ring strip is not effective in attracting the excited surface currents between the two antennas to decrease the coupling therebetween. For $a = 9$ and 10 mm, the S_{21} shows small differences. Hence, in this study, the smaller-size ring strip with $a = 9$ mm is selected.

Figure 11 shows the simulated S parameters of the two antennas with the isolation ring strip shorted to the ground plane using one shorting strip. In the proposed design, two shorting strips as shown in Figure 1 are used, and the S_{11} and S_{22} are generally the same as seen in Figure 4(a). However, in Figure 11, owing to only one shorting strip used, the obtained S_{11} and S_{22} are varied. The S_{21} in the upper band is also increased, as compared to the corresponding S_{21} shown in Figure 4(a). The obtained results indicate that the use of two shorting strips for short-circuiting the ring strip can lead to better results. It can also be concluded that the ring strip not only helps improve the impedance matching of the two antennas but also enhance the isolation therebetween.

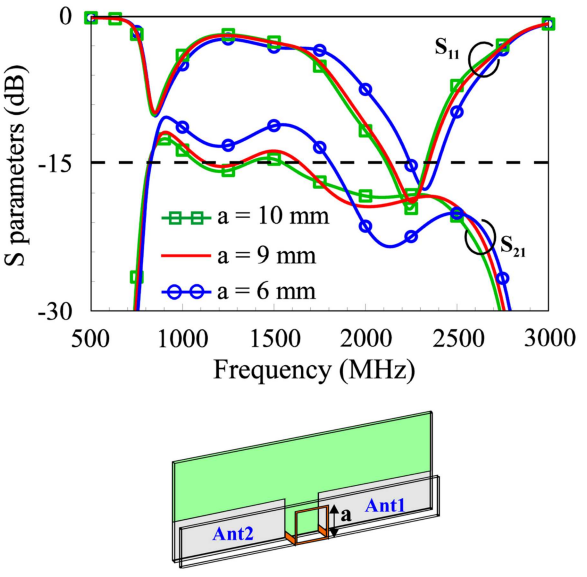

Figure 10 Simulated S parameters of the two antennas with the isolation ring strip of different sizes. [Color figure can be viewed in the online issue, which is available at wileyonlinelibrary.com]

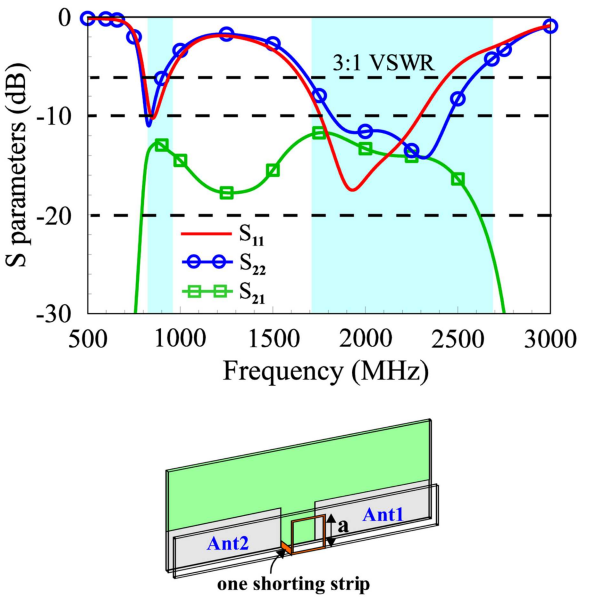

Figure 11 Simulated S parameters of the two antennas with the isolation ring strip shorted to the ground plane using one shorting strip. [Color figure can be viewed in the online issue, which is available at wileyonlinelibrary.com]

4. CONCLUSION

A WWAN/LTE antenna array comprising two small-size antennas and a ring strip embedded therebetween to achieve enhanced isolation between antennas and good antenna efficiency has been presented. The proposed antenna array can be mainly disposed on a small FR4 substrate of size 10 × 70 mm^2, making it easy to implement and also promising to be mounted at one edge (bottom edge in this study) of the smartphone. The two antennas have small size and can achieve multiband or wideband operation. The ring strip short-circuited to the system ground plane not only helps improve the impedance matching of the two antennas but also enhance the isolation therebetween. The fabricated prototype of the proposed design has been tested, and the desired operating bands (824–960/1710–2690 MHz) have been covered with good impedance matching. Good isolation with the S_{21} less than −15 dB over both bands has been achieved. The antenna efficiencies of about 40–52% and 50–90%, respectively, over the lower and upper bands have been obtained. The proposed antenna array is suitable for practical smartphone applications to achieve LTE MIMO operation or dual WWAN operation for dual-talk function.

REFERENCES

1. A. Diallo, C. Luxey, P. Le Thuc, R. Staraj, and G. Kossiavas, Study and reduction of the mutual coupling between two mobile phone PIFAs operating in the DCS1800 and UMTS bands, IEEE Trans Antennas Propag 54 (2006), 3063–3074.
2. G. Park, M. Kim, T. Yang, J. Byun, and A.S. Kim, The compact quad-band mobile handset antenna for the LTE700 MIMO

application, In Proceedings of the 2009 IEEE Antennas Propagation Society International Symposium, Charleston, SC.
3. H. Bae, F.J. Harackiewicz, M.J. Park, T. Kim, N. Kim, D. Kim, and B. Lee, Compact mobile handset MIMO antenna for LTE700 applications, Microwave Opt Technol Lett 52 (2010), 2419–2422.
4. A. Tatomirescu, M. Pelosi, M.B. Knudsen, O. Franek, and G.F. Pedersen, Port isolation method for MIMO antenna in small terminals for next generation mobile networks, In Proceedings of the 2011 IEEE Vehicular Technology Conference (VTC fall), San Francisco, CA.
5. R.A. Bhatti, S. Yi, and S.O. Park, Compact antenna array with port decoupling for LTE-standardized mobile phones, IEEE Antennas Wireless Propag Lett 8 (2009), 1430–1433.
6. N. Lopez, C. Lee, A. Gummalla, and M. Achour, Compact metamaterial antenna array for long term evolution (LTE) handset application, In Proceedings of the 2009 IEEE International Workshop on Antenna Technology (iWAT), Santa Monica, CA, pp. 1–4.
7. Y.S. Shin and S.O. Park, A monopole antenna with a magneto-dielectric material and its MIMO application for 700 MHz-LTE-band, Microwave Opt Technol Lett 52 (2010), 2364–2367.
8. J. Lee, Y.K. Hong, S. Bae, G.S. Abo, W.M. Seong, and G.H. Kim, Miniature long-term evolution (LTE) MIMO ferrite antenna, IEEE Antennas Wireless Propag Lett 10 (2011), 603–606.
9. Y.W. Chi and K.L. Wong, Quarter-wavelength printed loop antenna with an internal printed matching circuit for GSM/DCS/PCS/UMTS operation in the mobile phone, IEEE Trans Antennas Propag 57 (2009), 2541–2547.
10. K.L. Wong and S.C. Chen, Printed single-strip monopole using a chip inductor for penta-band WWAN operation in the mobile phone, IEEE Trans Antennas Propag 58 (2010), 1011–1014.
11. K.L. Wong, W.Y. Chen, and T.W. Kang, On-board printed coupled-fed loop antenna in close proximity to the surrounding ground plane for penta-band WWAN mobile phone, IEEE Trans Antennas Propag 59 (2011), 751–757.
12. F.H. Chu and K.L. Wong, Internal coupled-fed dual-loop antenna integrated with a USB connector for WWAN/LTE mobile handset, IEEE Trans Antennas Propag 59 (2011), 4215–4221.
13. K.L. Wong and Y.W. Chang, Internal WWAN/LTE handset antenna integrated with USB connector, Microwave Opt Technol Lett 54 (2012), 1154–1159.
14. K.L. Wong and P.W. Lin, Integration of monopole slot and monopole strip for internal WWAN handset antenna, Microwave Opt Technol Lett 54 (2012), 1718–1723.
15. K.L. Wong, T.W. Kang, and M.F. Tu, Antenna array for LTE/WWAN and LTE MIMO operations in the mobile phone, Microwave Opt Technol Lett 53 (2011), 1569–1573.
16. ANSYS HFSS, Ansoft Corp, Pittsburgh, PA. Available at http://www.ansys.com/products/hf/hfss/

OPTIMIZATION OF A BROADBAND VH LUMPED-ELEMENT FERRITE CIRCULATOR

Jacob R. Smith,[1] Hang Dong,[1] Jeffrey L. Young,[1] and Brandon Aldecoa[2]
[1] Department of Electrical and Computer Engineering, University of Idaho, Moscow, ID 83844-1024; Corresponding author: jyoung@uidaho.edu
[2] First RF, Boulder, CO

Received 19 February 2013

ABSTRACT: *A multistage optimization procedure is provided to maximize the operating bandwidth of a very high frequency circulator. We show through hardware validation that bandwidths on the order of 52.3–80.9 MHz are achievable using a 15 dB isolation specification. Simulation studies indicate that bandwidths on the order of 100% are possible, but such wideband performance has not been achieved in hardware to date. The optimization procedure uses both genetic algorithms and orthogonal sweep methods to find the best crossover geometry and ferrite properties, but the outcome of both methods is roughly the same. Matching networks are used to tune the response and to widen the operating frequency band. These networks are optimized using Pareto tradeoff charts in the context of power metrics like return loss, isolation, and insertion loss.* © 2013 Wiley Periodicals, Inc. Microwave Opt Technol Lett 55:1476–1481, 2013; View this article online at wileyonlinelibrary.com. DOI 10.1002/mop.27654

Key words: *circulators; bandwidth; ferrites; VHF; optimization*

1. INTRODUCTION

The concept of a lumped-element, crossover circulator for use in the very high frequency (VHF)–ultra-high frequency (UHF) range was pioneered by Konishi [1] in 1965. Since that time there have been numerous contributions to its underlying theory of operation and methods of fabrication [2–5]. However, there are still questions about maximum wideband operation for a given isolation specification. In the VHF range, marketed circulators tend to be narrowband, but this performance is not driven by physical limitations. The emergence of computational electromagnetic software in recent years has dramatically improved the way circulators can be designed. And, through the use of new, sophisticated methods of optimization and fabrication described herein, it is now possible to close the gap between the upper bound of theoretical performance and the performance of physical devices.

As experimentally verified with a fabricated VHF circulator, bandwidths on the order of 54.7% are physically possible using a novel design process. Simulation studies indicate that bandwidths can be as large as 100%, but parasitics not accounted for in simulation tend to limit actual hardware performance.

To achieve wideband performance, a multistage optimization methodology is utilized that exploits data obtained from both simulation and experiment. Due to the overwhelmingly large number of free design parameters (e.g., geometry values, material values, biasing value, and matching network values), it is neither practical nor insightful to attempt an optimization over the entire design space. Instead, we first focus on finding the optimal geometry and materials for the crossover network, then the optimal biasing field, and finally the optimal matching network. This methodology hinges on the notion of the circulation impedance and the knowledge it provides in estimating bandwidth—prior to matching network design—as described next.

By definition, the circulation impedance Z_c is the load impedance connected to a linear, nonreciprocal, three-port network that results in perfect isolation. It is also the impedance associated with perfect return loss and insertion loss if the network is lossless. Thus, the network, if lossless and nonreciprocal, is a perfect circulator when all three of its ports are loaded with Z_c. From standard network analysis, it can be shown that the circulation impedance is purely a function of the network's impedance parameters [6]:

$$Z_c = R_c + jX_c \equiv \frac{Z_{21}^2}{Z_{31}} - Z_{11}. \quad (1)$$

We may view the concept of the circulation impedance in terms of a nonreciprocal ferrite network loaded by matching networks. See Figure 1 for a network depiction and for the various impedance definitions used in this discussion. The role of the matching networks is to realize as closely as possible the frequency response of Z_c over some band of frequencies as viewed by the nonreciprocal network.